

Real-Time Wind Synthesis from Doppler Radar Observations during the Mesoscale Alpine Programme



M. Chong,^{*} J.-F. Georgis,⁺ O. Bousquet,[#] S. R. Brodzik,[#] C. Burghart,[@]
S. Cosma,⁺ U. Germann,[&] V. Gouget,^{*} R. A. Houze Jr.,[#] C. N. James,[#]
S. Prieur,⁺ R. Rotunno,[@] F. Roux,⁺ J. Vivekanandan,[@] and Z.-X. Zeng[#]

ABSTRACT

A real-time and automated multiple-Doppler analysis method for ground-based radar data, with an emphasis on observations conducted over complex terrain, is presented. It is the result of a joint effort of the radar groups of Centre National de Recherches Météorologiques and Laboratoire d'Aérodynamique with a view to converging toward a common optimized procedure to retrieve mass-conserved three-dimensional wind fields in the presence of complex topography. The multiple-Doppler synthesis and continuity adjustment technique initially proposed for airborne Doppler radar data, then extended to ground-based Doppler radars and nonflat orography, is combined with a variational approach aimed at improving the vertical velocity calculation over mountainous regions. This procedure was successfully applied in real time during the Mesoscale Alpine Programme Special Observing Period. The real-time processing and display of Doppler radar data were intended to assist nowcast and aircraft missions, and involved efforts of the United States, France, and Switzerland.

1. Introduction

One of the main objectives of the Mesoscale Alpine Programme (MAP) special observing period (SOP; 7 September–15 November 1999) was to investigate the mechanisms of orographically generated and/or controlled heavy precipitation events with spe-

cial emphasis on their dynamics, microphysics, and hydrological consequences (see Bougeault et al. 1998). In this context, the French RONSARD research radar was operated in coordination with the Swiss Meteorological Agency (SMA) operational radar at Monte Lema to obtain dual-Doppler data. In addition to the real-time processing and display of reflectivity and Doppler velocity over the complex terrain of MAP with the MountainZebra system (James et al. 2000), a dual-Doppler synthesis was performed to obtain the three-dimensional (3D) wind fields. This paper aims at presenting this unique real-time application carried out in the field during MAP, with intent to assist nowcast and aircraft guidance. Recently, analysis efforts were made to provide 3D wind fields in a real-time context from multiple-Doppler radar data. Wurman (1994) and Satoh and Wurman (1999) proposed to use a bistatic multiple-Doppler radar system on a beam-by-beam, gate-by-gate basis. Protat and Zawadzki (1999) also used such a radar network but proposed a variational method to retrieve the wind components in a Cartesian grid.

To retrieve mass-conserved 3D wind fields from ground-based or airborne multiple-Doppler observa-

^{*}Centre National de Recherches Météorologiques, CNRS and Météo-France, Toulouse, France.

⁺Laboratoire d'Aérodynamique, CNRS and Université Paul Sabatier, Toulouse, France.

[#]Department of Atmospheric Sciences, University of Washington, Seattle, Washington.

[@]National Center for Atmospheric Research, ** Boulder, Colorado.

[&]MeteoSvizzera, Locarno-Monti, Switzerland.

**The National Center for Atmospheric Research is sponsored by the National Science Foundation.

Corresponding author address: Dr. Michel Chong, CNRM (CNRS and Météo-France), 42 Av. Coriolis, 31057 Toulouse Cedex, France.

E-mail: chong@meteo.fr

In final form 9 June 2000.

©2000 American Meteorological Society

tions over mountainous regions, Georgis et al. (1999, hereafter referred to as GRH) developed a new technique which, for the first time, explicitly took the orographic effects into account. In this approach, the horizontal wind components were first derived from the Doppler measurements, then the vertical component was deduced from the integration of the air mass continuity equation, expressed as a variational problem so as to fit the boundary conditions and additional constraints. However, such a technique has to be applied only to data collected at low-elevation angles ($\leq 45^\circ$) in order to mitigate the contribution of the vertical hydrometeor fall speed to the observed Doppler velocities. Furthermore, because the horizontal wind components have to be determined from two noncolinear Doppler velocity measurements, it is not possible to obtain information about the kinematic structure in regions close to the radar baseline.

The multiple-Doppler synthesis and continuity adjustment technique (MUSCAT), which was developed to recover wind components from airborne Doppler data (Bousquet and Chong 1998, hereafter referred to as BC) and ground-based radar observations (Chong and Bousquet 2000, manuscript submitted to *Meteor. Atmos. Phys.*), permitted overcoming these limitations by providing a simultaneous solution for the three wind components. MUSCAT, which could only be applied to flat terrain in its initial form, was recently adapted by Chong and Cosma (2000, hereafter referred to as CC) to handle the presence of complex topography. However, because of the least squares solution for the continuity equation and a lack of Doppler velocity measurements at high-elevation angles, the vertical wind component is not always as well retrieved as the horizontal wind field.

Hence, we propose to calculate the horizontal wind components via MUSCAT, since this technique allows a reliable wind retrieval on a significantly enlarged domain, then to deduce the vertical component through the variational technique developed by GRH in order to derive 3D wind fields from the integration of the air mass continuity equation. Section 2 reviews the two wind synthesis methods of this two-step real-time and automated multiple-Doppler analysis method (RAMDAM), which benefits from the best performances of each of them. The real-time procedure of RAMDAM is described in section 3, and section 4 shows some of the results obtained during the MAP SOP.

2. Wind synthesis methods

a. The MUSCAT algorithm for the determination of the horizontal wind

The basic principle of MUSCAT (BC) is a simultaneous solution of the three Cartesian wind components (u, v, w) from at least a pair of Doppler observations. Its formalism, built upon a two-dimensional framework that yields plane-to-plane variational analyses, consists of the minimization, in a least squares sense, of the following cost function:

$$F(u, v, w) \quad (1)$$

$$= \int_S [A(u, v, w) + B(u, v, w) + C(u, v, w)] dx dy,$$

where S is the horizontal domain at the considered altitude where Doppler observations are available; and $u, v,$ and w are solutions of

$$\frac{\partial F}{\partial u} = 0, \quad \frac{\partial F}{\partial v} = 0, \quad \frac{\partial F}{\partial w} = 0. \quad (2)$$

In (1), terms A, B, and C are cost functions quantifying the square values of the difference between the Doppler velocities and those deduced from the calculated wind components, of the anelastic continuity equation, and of the small-scale variations of the wind components, respectively.

The cost function A for the Doppler adjustment at a grid point is written as

$$A(u, v, w) \quad (3)$$

$$= \frac{1}{N} \sum_{i=1}^N \omega_i [\alpha_i u + \beta_i v + \gamma_i (w + v_T) - V_i]^2,$$

where v_T is the mean terminal particle fall speed estimated from the observed radar reflectivity; subscript i defines the i th observation that contributes to the gridpoint estimate; N is the number of observations; V is the measured radial velocity; and $\alpha, \beta,$ and γ are the direction cosines, in the $x, y,$ and z directions, respectively, of the radar beam. The ω is a Cressman distance-dependent weight function to account for noncollocated data and gridpoint values, permitting the interpolation of the polar coordinate radar data onto the Cartesian grid of interest to be included into the data fit. Bousquet and Chong (1998) noted that a separate

interpolation would create a sampling problem at short ranges, since it produces average Doppler velocity vectors from quite different directions. Incorporating the necessary interpolation into the least squares data adjustment allows the technique to take into account all the available observed velocities with their actual orientation.

The adjustment of the continuity equation [cost function B in (1)] is expressed within a grid cell as

$$B(u, v, w) = (FU + FV + FW)^2, \quad (4)$$

where FU , FV , and FW are the mass transported by u , v , and w wind components through the surfaces normal to x , y , and z , respectively. This flux formulation (CC) is more suitable to solve the problem of the orography-induced circulation (slope winds) in the MUSCAT variational analysis. It is expressed for individual grid boxes located between two successive horizontal planes, allowing a bottom-to-top plane-to-plane analysis since the wind components at the lower plane are supposed to be already calculated. It has the advantage of applying to either flat or complex terrain without explicitly evaluating the vertical velocity at the surface, since no mass transport exists through this rigid boundary. The lateral mass transports are evaluated according to the size of the lateral faces of the grid box intercepted by the topography.

Finally, the low-pass filtering of small-scale horizontal variations of u , v , and w [cost function C in (1)] is realized through the minimization of the second-order derivatives. Here, C is expressed as

$$C(u, v, w) = J_2(u) + J_2(v) + J_2(w), \quad (5)$$

with $J_2 = (\partial^2/\partial x^2)^2 + 2(\partial^2/\partial x\partial y)^2 + (\partial^2/\partial y^2)^2$. It is controlled by a weighting factor depending on the cutoff wavelength.

b. The variational determination of the vertical wind component

Using the MUSCAT-derived horizontal wind components, an a posteriori evaluation of the vertical velocity is obtained through an upward integration of the air mass continuity equation, as

$$\rho w = \rho_s w_s - \int_{z_s}^z \rho \left(\frac{\partial u}{\partial x} + \frac{\partial v}{\partial y} \right) dz, \quad (6)$$

where subscript s refers to the surface, and ρ is the air density depending on the altitude. The surface altitude $z_s(x, y)$ is derived from a digital terrain map and is used to define the vertical wind component $w_s(x, y)$ at the surface level as

$$w_s(x, y) = u_s(x, y) \frac{\partial z_s}{\partial x} + v_s(x, y) \frac{\partial z_s}{\partial y}, \quad (7)$$

where $u_s(x, y)$ and $v_s(x, y)$ are the horizontal wind components extrapolated down to the surface from the two lowest levels where u and v are available. This extrapolation relies on a mean vertical wind shear determined from these levels.

The a posteriori integration of the continuity equation is required by the fact that the three-dimensional wind field deduced from MUSCAT in the least squares sense does not strictly satisfy the mass conservation. However, extrapolating the surface wind components $u_s(x, y)$ and $v_s(x, y)$ in (7) from the data observed above may be a source of errors in the integration process. In addition, divergence error accumulation and density stratification contribute to the well-known numerical instability, which then needs to be substantially reduced. The approach proposed by GRH is based on corrections of the horizontal wind components, and subsequently the vertical velocity. The divergent part of the horizontal wind field is modified by adding to the u and v components a term constant with altitude, which derives from a scalar velocity potential $\phi(x, y)$, such as

$$u^* = u + \partial\phi/\partial x \quad (8)$$

$$v^* = v + \partial\phi/\partial y, \quad (9)$$

where superscript $*$ stands for the modified components. Then, the associated vertical velocity w^* can be readily written as

$$\rho w^* = \rho w + \rho_s (\nabla_h z_s \cdot \nabla_h \phi) - \nabla_h^2 \phi \int_{z_s}^z \rho dz, \quad (10)$$

where ∇_h is the horizontal del operator.

The velocity potential $\phi(x, y)$ is determined through a variational analysis that minimizes the horizontal gradients of vertical velocity w^* within the 3D domain of interest (D) and the vertical velocity w^*_{top} at the upper boundary, according to the following cost function:

$$J_\phi = \int_{S_{\text{top}}} \lambda (w^*_{\text{top}})^2 + \mu \int_D \left[\left(\frac{\partial w^*}{\partial x} \right)^2 + \left(\frac{\partial w^*}{\partial y} \right)^2 \right] dx dy dz, \quad (11)$$

where S_{top} denotes the top-level surface, λ is a variable weight aimed at modulating the minimization of w^*_{top} according to the reflectivity value measured at the top, and μ is a normalizing factor ensuring that both integrals involved in the cost function (11) have the same relative weight. We will refer to GRH for the full expression of (11) in terms of the velocity potential $\phi(x, y)$, using (10). The variational adjustment of ϕ , hence w^* , resembles that proposed by Chong and Testud (1983), who first introduced the concept of minimizing the horizontal gradients of w^* in order to force the vertical velocity field to be as regular as possible in the mathematical sense.

3. Real-time procedure

During the Wet MAP intensive observation period (IOP), a great challenge consisted of obtaining information about microphysical and kinematic characteristics of the observed precipitating systems in real time. The motivation for developing real-time wind analysis capabilities was to contribute to nowcasting purposes and also to aircraft missions. Documentation of the precipitation and airflow structure was important to help select the best region to be sampled by the airborne Doppler radars involved in MAP. The real-time retrieval of mass-conserved 3D wind fields was realized over the Lago Maggiore target area, using the dual-Doppler observations conducted with the French RONSARD C-band research radar at San Pietro-Mosezzo (45.460°N, 8.517°E, 155-m altitude) nearly 60 km west of Milan, Italy, and the Swiss op-

erational C-band radar of Monte Lema (46.042°N, 8.833°E, 1625-m altitude). The distance between the two radars was about 70 km. Figure 1 shows their implementation in the observational area, along with the other research radars involved in MAP SOP. In particular the National Center for Atmospheric Research (NCAR) S-Pol (polarimetric) Doppler radar located at Vergiate, Italy, (45.720°N, 8.730°E, 280-m altitude) could monitor the 3D precipitation and microphysical structure within the broadscale dual-Doppler coverage provided by the Swiss and French radars. The S-Pol radar also provided Doppler measurements to enhance the Doppler data resolution in the central portion, but they were not used in the real-time wind synthesis during the MAP SOP. The U.S. X-band Doppler radar on wheels, with three possible locations, was dedicated to observe the precipitation and airflow structure within the major Toce and Ticino

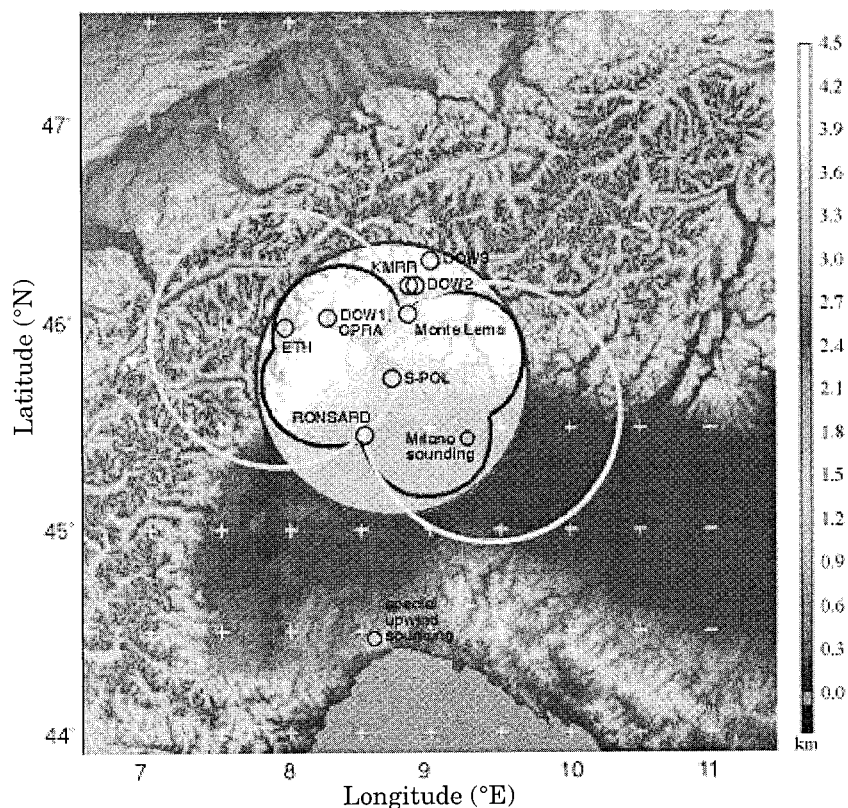


FIG. 1. Locations of the ground-based dual-Doppler and polarimetric radar observations during the MAP SOP. The RONSARD and Monte Lema radars are C-band radars for dual-Doppler observations, while the S-Pol radar, midway between these radars, is the S-band polarimetric Doppler radar for deducing the microphysical structure of precipitation. Details of the topography are represented. The large circles on either side of the RONSARD–Monte Lema baseline define the dual-Doppler array. The large circle centered on the S-Pol radar encloses the region of high-resolution polarimetric radar data (from Houze et al. 1998).

River valleys that could not be investigated by the above-mentioned research radars. Details of the ground-based radar operation modes can be found in the MAP implementation plan (Binder et al. 1999; available online at <http://www.map.ethz.ch>).

The Monte Lema scanning mode (Joss et al. 1998) was composed of two interleaved volume scans, each consisting of 10 360° azimuth sweeps performed in 2.5 min, with azimuthal resolution of 1.0° and gate spacing of 83 m. Twelve contiguous gates were processed to obtain a 1-km radial resolution over a maximum range of 130 and 230 km for Doppler and reflectivity measurements, respectively. The first set of elevation angles at -0.3°, 1.5°, 3.5°, 5.5°, 7.5°, 9.5°, 13.0°, 18.3°, 25.3°, and 34.5° was followed by a second set at 0.5°, 2.5°, 4.5°, 6.5°, 8.5°, 11.0°, 15.5°, 21.6°, 29.6°, and 40.0°. Three different Nyquist velocities were used: 8.27 m s⁻¹ for the four lowest elevations, followed by 11.0 m s⁻¹ for the four next intermediate elevations, and 16.5 m s⁻¹ for the remaining higher-elevation sweeps. The complete high-resolution scan was realized in 5 min; data were saved as pseudo-GIF (graphics interchange format) images; and the procedure was repeated continuously. The RONSARD operation mode also consisted of a sequence of 20 360° azimuth sweeps obtained in ~10 min, with azimuthal resolution of 0.62° and gate spacing of 200 m over a maximum range of 102.4 km. Elevation angles are 0.62°, 1.23°, 1.85°, 2.46°, 3.08°, 3.69°, 4.31°, 4.92°, 5.54°, 6.15°, 6.77°, 7.38°, 8.35°, 9.67°, 11.43°, 13.89°, 17.75°, 24.35°, 37.71°, and 69.43° from the horizontal. The RONSARD radar, which had a Nyquist velocity of 19.6 m s⁻¹, was operated in coordination with the Monte Lema radar on a 15-min cycle. For real-time purpose, data from the RONSARD radar were degraded; that is, for each sweep only every fourth range gate and every other ray were sent as pseudo-GIF images to the Project Operation Centre (POC) at Milano Linate military airport, where RAMDAM was run. Note, however, that the radial resolution was doubled at the five highest sweeps.

Figure 2 presents the schematic data flow of the Monte Lema, RONSARD, and S-Pol radars, and the data processing from the French and U.S. components, as described in the U.S. Wet MAP

operations plan (available online at <http://www.atmos.washington.edu/gcg/MG/MAP/map.opsplan.html>). In the following, we focus on the RAMDAM processing chain (central part of Fig. 2), done on a PC-LINUX machine. Every 15 min, the pseudo-GIF files of reflectivity and Doppler data received from each radar at POC (through a dedicated Internet line for Monte Lema and an ISDN line for RONSARD) were decoded and combined into local binary files. A first step of RAMDAM was to dealias the Doppler velocities, according to the velocity–azimuth display (VAD)–based method proposed by Yamada and Chong (1999), which consisted of finding the Nyquist interval number from the zeroth order of the VAD Fourier expansion, without requiring external information such as an environmental wind profile. These authors found that such determination yielded correct dealiasing as long as, at a given radial distance, Doppler velocity data were available within an azimuthal interval larger than 160°. A more sophisticated technique (James and Houze 2000, manuscript submitted to *J. Atmos. Oceanic Technol.*) was also available during MAP to dealias Monte Lema radial velocity measurements with a Nyquist velocity as low as 8.27 m s⁻¹. The dealiasing was accomplished using

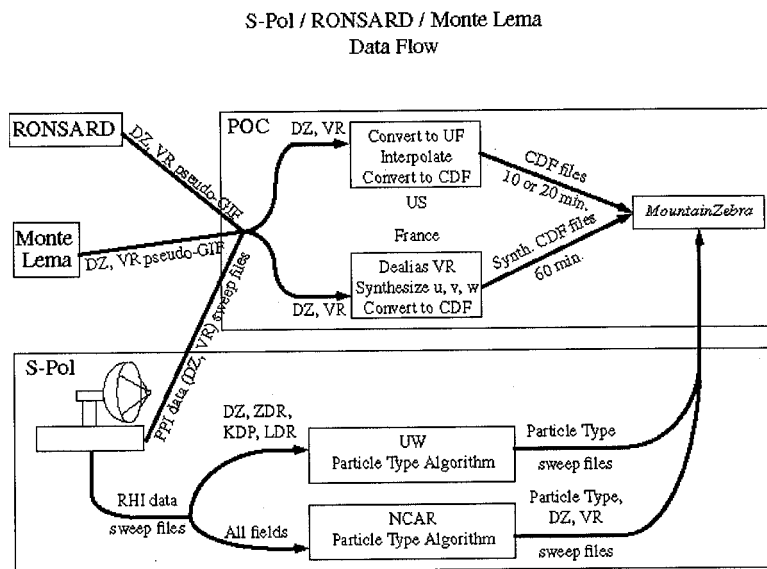


FIG. 2. Schematic data flow of the S-Pol, RONSARD, and Monte Lema radars involved in the Lago Maggiore target area. Reflectivity and Doppler velocity data are concentrated at the POC, and processed through the U.S.- and French-specific software, before their visualization by MountainZebra. The S-Pol radar was also operated in RHI (vertical plane) scan with the polarimetric mode in order to provide the microphysical structure of precipitation, using two differentiated algorithms (Zeng et al. 2000, manuscript submitted to *J. Appl. Meteor.*; Vivekanandan et al. 1999) from the University of Washington (UW) and NCAR.

both temporal and spatial continuity, and required a last processed Doppler volume, a velocity–azimuth display profile, or a sounding profile. The dealiased data from Monte Lema radar were then combined with the corresponding RONSARD data into the two-step multiple-Doppler wind synthesis as described in section 2. Finally, the resulting 3D wind and reflectivity fields were written into Unidata’s Network Common Data Format files to be compatible with the MountainZebra system developed by the University of Washington (James et al. 2000) and dedicated to multiple-origin data processing and visualization over complex terrain. The real-time processing took approximately 15–20 min. (Note that the 60-min cycle indicated in Fig. 2 was a tentative schedule at the time of specifying the Wet MAP operations plan.)

4. Application to MAP data

In this section, we present three different cases of dual-Doppler observations during the MAP SOP. The aim is not to provide a complete description of the observed precipitating system but only to illustrate the reliability of the RAMDAM procedure.¹ During the MAP SOP, 3D wind fields were retrieved within a domain of 147 km × 147 km × 11 km, with a grid resolution of 3 km × 3 km

¹A description of the observations that is duplicated from the POC Science Director notes (i.e., Prof. R. A. Houze Jr. and Dr. R. Rotunno), as well as figures below, are available on the MAP data catalog online at <http://www.joss.ucar.edu/map/catalog/>, provided by the University Corporation for Atmospheric Research Joint Office for Science Support. This catalog will be duplicated on a CD-ROM support, and all data will be available through the MAP Data Centre, Zurich, Switzerland. The most up-to-date versions of the POC science summaries can be found online at http://www.atmos.washington.edu/gcg/MG/MAP/iop_summ.html maintained by Houze. Note also that an overview of the special observing period of MAP will be found in Bougeault et al. (2000).

× 0.5 km. The retrieval domain was centered on the S-Pol radar. The relatively coarse grid resolution was used to take into account the substantial low resolution of the RONSARD data transmitted to the POC. Of course, using data at full resolution (and also Doppler data from the S-Pol radar) will permit finer horizontal and vertical meshes in postmortem MAP SOP analyses. The horizontal and vertical influence radii of the Cressman weighting function used in the MUSCAT formalism (1) were set, respectively, to 3.0 and 1.2 km, while the low-pass filter was such that the cutoff wavelength was 4 times the horizontal grid resolution.

a. IOP 2A: Squall line over the Lago Maggiore

In the afternoon and evening of 17 September 1999, a major squall line developed over the mountains to the northwest of Lago Maggiore and moved over the dual-Doppler lobes of the RONSARD and Monte Lema radars. It occurred in a convectively unstable flow well ahead of a long-wave trough moving into western Europe. Figure 3 shows the dual-Doppler winds computed from the Monte Lema and RONSARD

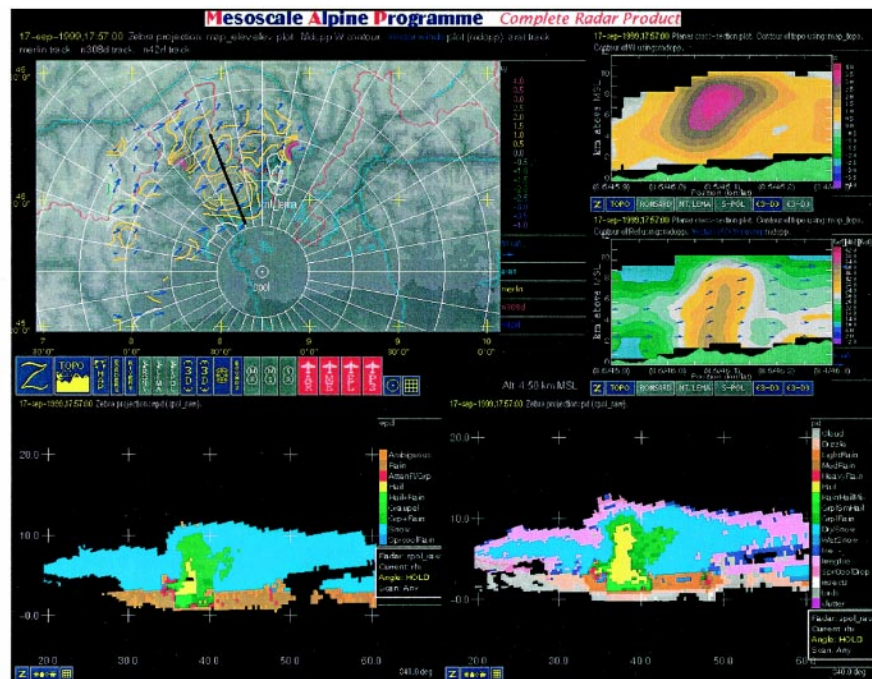


FIG. 3. MountainZebra visualization of three-dimensional wind fields (upper panels, blue arrows) from RONSARD and Monte Lema radar data, and particle-type distribution from S-Pol data (lower panels), at 1757 UTC 17 Sep 1999. The upper-left panel shows the horizontal wind vectors and the vertical velocity pattern at 4.5-km altitude, along with the background topography. The heavy black line at 340° from S-Pol indicates the position of the vertical cross section of vertical velocity, wind vectors and reflectivity (upper right panels), and of particle types using the UW algorithm (lower-left panel) and the NCAR algorithm (lower-right panel).

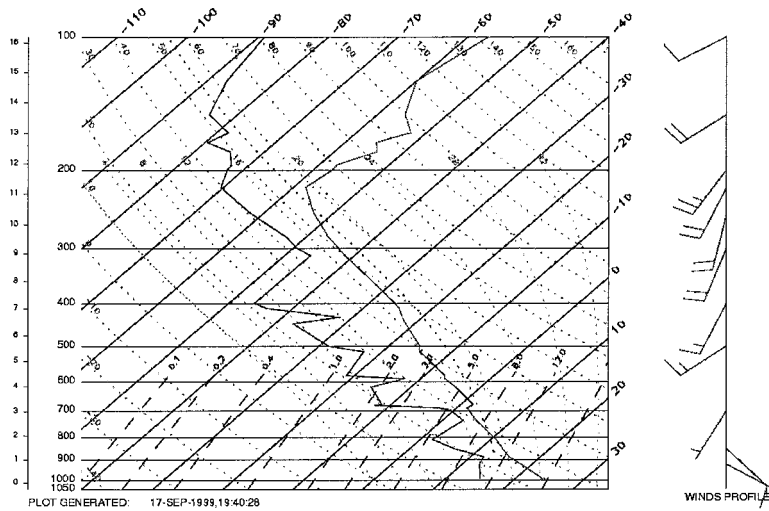


FIG. 4. SkewT–logp diagram and wind profile, deduced from the Milan sounding at 1800 UTC 17 Sep 1999.

Doppler radars (upper panels) along with the real-time analysis of the S-Pol radar data for the microphysical structure of precipitation particles (lower panels), at 1757 UTC 17 September 1999. The orientation of the squall line was mainly southwest–northeast. The retrieved horizontal flow at 4.5-km altitude (upper left panel) was essentially southwesterly, and was consistent with the 1800 UTC sounding launched at Milan (Fig. 4), which also revealed the convective character of the atmosphere in this early season IOP 2A. It is worth noting that the pattern of the vertical velocity in the vertical cross section (along 340° from S-Pol) was well correlated with the pattern of observed reflectivity (see the upper-right panels). In particular, the highest reflectivity values within the observed convective cell were associated with the strongest upward motions (up to 3.5 m s⁻¹) where, according to the S-Pol data (lower panels), water vapor was condensed and transformed into hail and snow aggregates.

b. IOP 8: Persistent lifting of stable air during a frontal passage

During IOP 8 that occurred between 19 and 21 October 1999, a frontal cloud band moved eastward over northern Italy and was stalled over the Lago Maggiore region so that a large and persistent area of stratiform precipitation was observed from 0400 to 1600 UTC 21 October 1999. Figure 5 shows the dual-Doppler winds and the reflectivity pattern at 2 km, deduced from the Monte Lema and RONSARD radar data collected at 0815 UTC. The retrieved strong southeasterly flow (upper panel) was nearly perpendicular to the mountains on the west side of the Lago Maggiore region, and was consistent in intensity and direc-

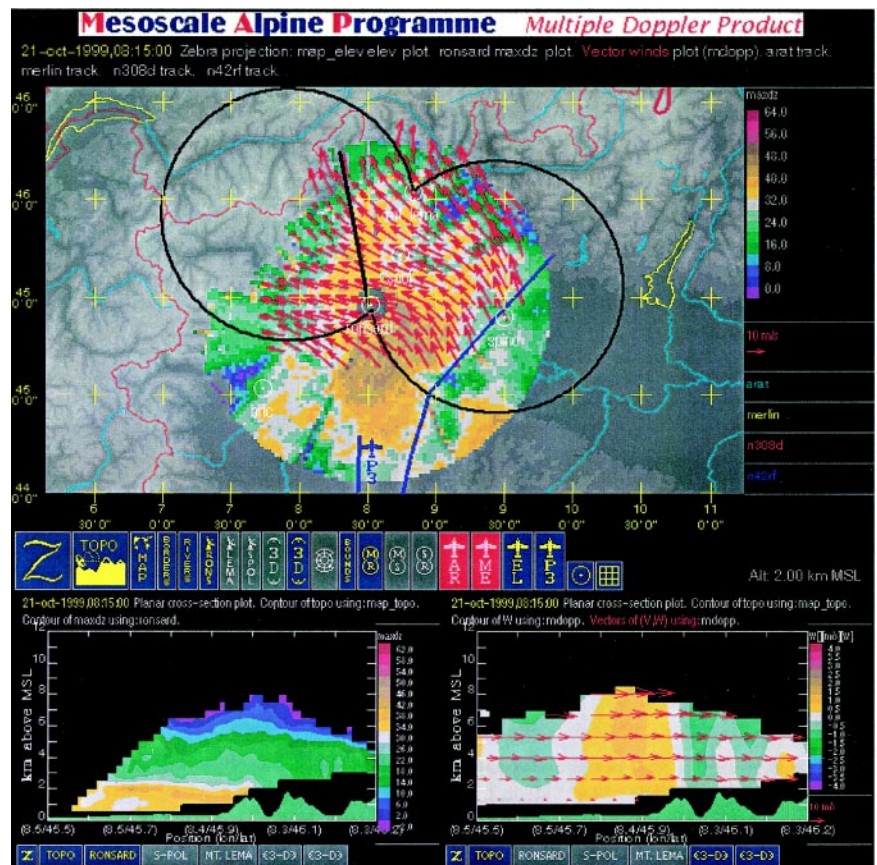


FIG. 5. MountainZebra visualization of wind field (red arrows) at 0815 UTC 21 Oct 1999. The upper panel represents the airflow at 2-km altitude, with superimposed reflectivity pattern from RONSARD. Also indicated are the dual-Doppler lobes (black circular arcs) from RONSARD and Monte Lema radars. The lower panel is the nearly northward vertical cross section (from RONSARD) of reflectivity (left), wind vectors and vertical velocity (right).

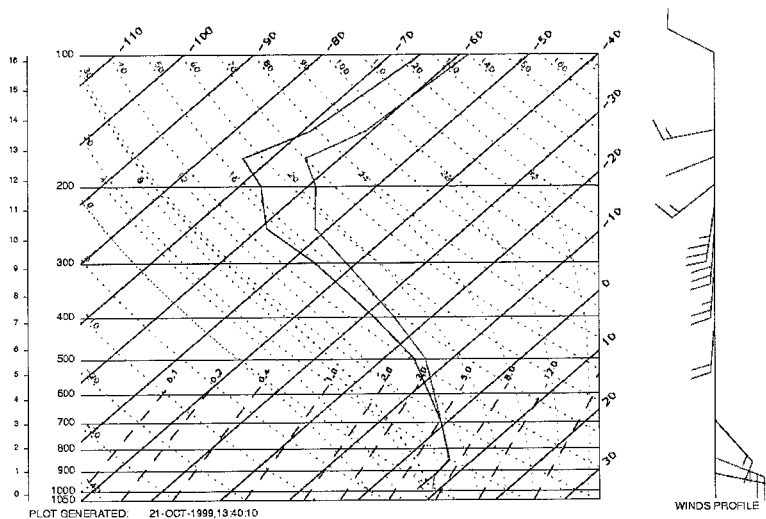


FIG. 6. As in Fig. 4, but for the sounding at 1200 UTC 21 Oct 1999.

tion with the Milan sounding at 1200 (Fig. 6) and the 850 hPa wind forecast at 1200 (Fig. 7) from the Canadian Mesoscale Compressible Community (MC2) nonhydrostatic model (Benoit et al. 1997). The MC2 model was initialized at 2100 UTC 20 October 1999. As noted in the POC Science Director notes, there was

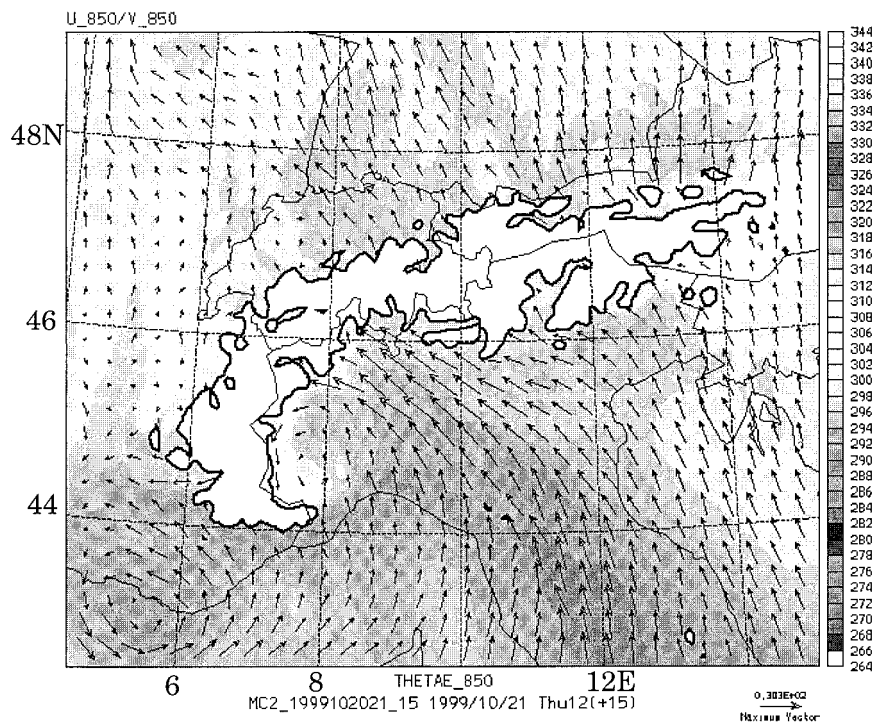


FIG. 7. Forecast of equivalent potential temperature (grayscale) and horizontal airflow at 850 hPa, 1200 UTC 21 Oct 1999, as derived from the MC2 model. The white region encloses mountains above 850 hPa.

a suggestion in the data of a vortex farther to the southwest, in agreement with the model forecast. The lower panels, which show a nearly northward vertical cross section across the RONSARD radar, indicate the stratiform character of the precipitation (lower left image) within an extremely stable air and associated with moderate upward motions ($\leq 1.5 \text{ m s}^{-1}$; lower right panel) occurring on the upwind slopes of the mountains. Downward motions also appeared on the downwind slopes.

c. IOP 9: Stratiform precipitation in frontal system passing rapidly over northern Italy

IOP 9 was activated during 21 and 23 October 1999 and also concerned a frontal cloud system, but this one moved rapidly across northern Italy. Radar observations were performed in the late afternoon of 22 October until the afternoon of 23 October 1999. Figure 8 gives an example of dual-Doppler wind synthesis at 0630 UTC 23 October. The horizontal flow at 2-km altitude (upper panel)

was mostly from the southwest and underwent cyclonic rotation as it approached the mountains. This was in contrast with the two cases previously presented, which exhibited different flow regimes. Again, the southwesterly flow was consistent with the winds from the 0600 UTC Milan sounding (not shown). This sounding showed stable air at low levels. Despite the differences in the flow regimes, the vertical structure along the north-south cross section through the RONSARD radar (lower panel) was comparable with that of the IOP 8 case (Fig. 5), with clear evidence of stratiform features in both precipitation structure and mesoscale vertical motion. This suggests that the quality of the wind synthesis does not depend on the direction of the flow.

5. Conclusions

The real-time and automated multiple-Doppler analysis method (RAMDAM) jointly developed by Centre National de Recherches Météorologiques and Laboratoire d'Aérodynamique has been presented. It has been proposed to deduce three-dimensional wind and reflectivity fields from ground-based dual-Doppler radar observations conducted over the complex terrain of the MAP SOP. RAMDAM is a processing chain that accounts for the main steps of Doppler data analysis: dealiasing and wind synthesis. The dealiasing procedure proposed by Yamada and Chong (1999) was used for the RONSARD radar data: it is based on the determination of the Nyquist interval number used to correct the Doppler velocities, through a Fourier analysis of the azimuthal data distribution at a specified distance from the radar. For Monte Lema radar data, the dealiasing technique by James and Houze (2000, manuscript submitted to *J. Atmos. Oceanic Technol.*) was preferred since it was more suitable for low Nyquist velocity. The wind synthesis in RAMDAM combines the best performances of two approaches in a two-step procedure: the MUSCAT algorithm developed by BC and Chong and Bousquet (2000, manuscript submitted to *Meteor. Atmos. Phys.*) for airborne and ground-based radars, and its subsequent modification for complex terrain (CC); and the variational technique by GRH in order to derive 3D wind fields satisfying the mass conservation.

Examples of application of RAMDAM during the MAP SOP have been used as illustrations. The three cases of dual-Doppler observations during IOPs 2A, 8, and 9 have clearly shown the ability of RAMDAM to provide the wind structure over the complex Alpine mountains. The IOP 2A was more convective than the IOPs 8 and 9. The wind syntheses concerned the convective circulation associated with a squall line (IOP 2A), and the mesoscale flow within the stratiform precipitation systems of IOPs 8 and 9, with different pre-

vailing wind directions over the Lago Maggiore target area. The obtained airflow structures were found to be consistent with the Milan sounding data and also the wind forecast from a fine-mesh mesoscale model. Finally, the postmortem SOP analyses planned for ground-based and/or airborne Doppler radar observations will benefit from the RAMDAM performances, with full resolution and the possibility to combine data from additional radars (e.g., S-Pol and the airborne Doppler radars).

Acknowledgments. The Mesoscale Alpine Programme was an international cooperative field experiment, involving Austria, Canada, Croatia, France, Germany, Great Britain, Greece, Hungary, Italy, Slovakia, Slovenia, Spain, Switzerland, and the United States. It was made possible thanks to the commitment of all participants from each country. The French contribution was mainly supported by INSU/PATOM (Programme Atmosphère et Océan à Moyenne Echelle) and Météo-France, with additional support from Centre National d'Etudes Spatiales and Electricité de France. We are indebted to Dr. Jürg Joss, who suggested the implementation of the real-time wind analysis from the Monte Lema and RONSARD radars, and to Dr. Gianmario Galli for providing us with information about GIF image decoding. We are also indebted

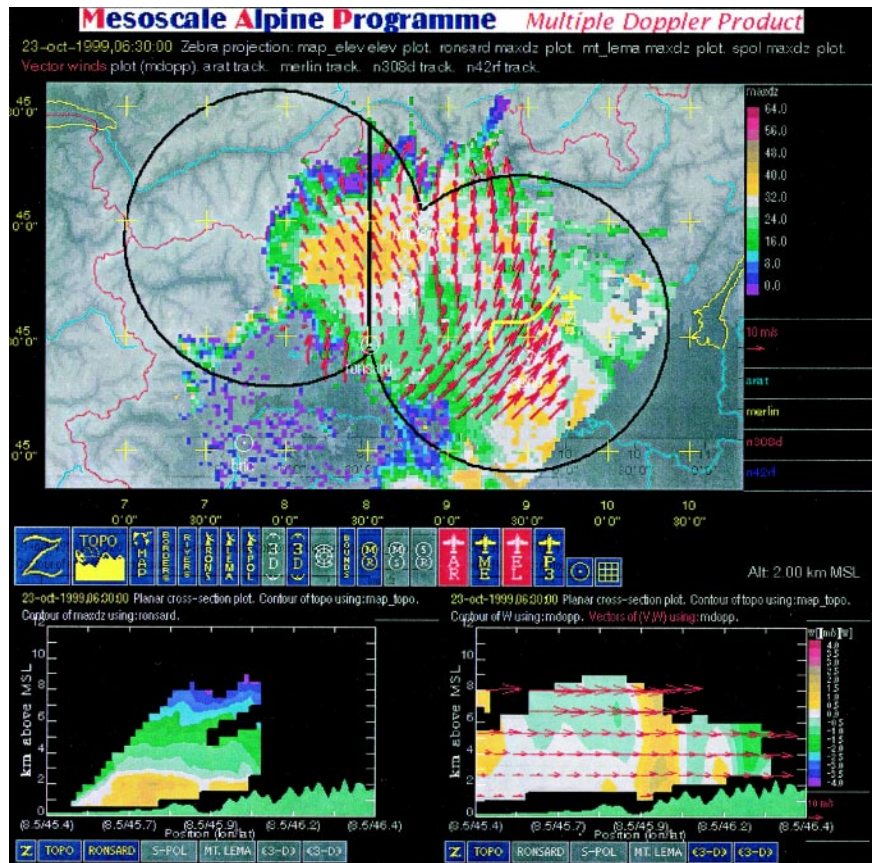


FIG. 8. As in Fig. 5, but for 0630 UTC 23 Oct 1999. The reflectivity pattern in the upper panel is a composite from Monte Lema, S-Pol, and RONSARD radars.

to the technical and scientific teams (among whom are R. Riguet and Dr. G. Scialom) that have been devoted to the RONSARD radar operations.

References

- Benoit, R., M. Desgagné, P. Pellerin, S. Pellerin, Y. Chartier, and S. Desjardins, 1997: The Canadian MC2: A semi-Lagrangian, semi-implicit wideband atmospheric model suited for finescale process studies and simulation. *Mon. Wea. Rev.*, **125**, 2382–2415.
- Binder, P., A. Rossa, P. Bougeault, J. Moore, D. Jorgensen, and M. Bolliger, 1999: Mesoscale Alpine Programme: Implementation plan, Version 4.1 260 pp. [Available from MAP Data Centre, ETH, Zürich, CH-8093, Switzerland.]
- Bougeault, P., P. Binder, and J. Kuettner, 1998: MAP Science Plan. 64 pp. [Available from MAP Data Centre, ETH, Zürich, CH-8093, Switzerland.]
- , and Coauthors, 2000: The MAP special observing period. *Bull. Amer. Meteor. Soc.*, in press.
- Bousquet, O., and M. Chong, 1998: A multiple-Doppler synthesis and continuity adjustment technique (MUSCAT) to recover wind components from Doppler radar measurements. *J. Atmos. Oceanic Technol.*, **15**, 343–359.
- Chong, M., and J. Testud, 1983: Three-dimensional wind field analysis from dual-Doppler radar data. Part III: The boundary condition: An optimum determination based on a variational concept. *J. Climate Appl. Meteor.*, **22**, 1227–1241.
- , and S. Cosma, 2000: A formulation of the continuity equation of MUSCAT for either flat or complex terrain. *J. Atmos. Oceanic Technol.*, in press.
- Georgis, J.-F., F. Roux, and P. H. Hildebrand, 1999: Observation of precipitating systems over complex orography with meteorological Doppler radars: A feasibility study. *Meteor. Atmos. Phys.*, **72**, 185–202.
- Houze, R. A., Jr., J. Kuettner, and R. B. Smith, 1998: Mesoscale Alpine Programme. U.S. overview document and experiment design. 101 pp. [Available from MAP U.S. Project Office, UCAR/JOSS, P.O. Box 3000, Boulder, CO 80307-3000.]
- James, C. N., S. R. Brodzik, H. Edmon, R. A. Houze Jr., and S. E. Yuter, 2000: Radar data processing and visualization over complex terrain. *Wea. Forecasting*, **15**, 327–338.
- Joss, J., and Coauthors, 1998: Operational use of radar for precipitation measurements in Switzerland. ETH Zurich Final Rep. NRP 31, 108 pp.
- Protat, A., and I. Zawadzki, 1999: A variational method for real-time retrieval of three-dimensional wind field from multiple-Doppler bistatic radar network data. *J. Atmos. Oceanic Technol.*, **16**, 432–449.
- Satoh, S., and J. Wurman, 1999: Accuracy of composite wind fields derived from a bistatic multiple-Doppler radar network. Preprints, *29th Int. Conf. on Radar Meteorology*, Montreal, PQ, Canada, Amer. Meteor. Soc., 221–224.
- Vivekanandan, J., D. S. Zmic, S. M. Ellis, R. Oye, A. V. Ryzhkov, and J. Straka, 1999: Cloud microphysics retrieval using S-band dual-polarization radar measurements. *Bull. Amer. Meteor. Soc.*, **80**, 381–388.
- Wurman, J., 1994: Vector winds from a single-transmitter bistatic dual-Doppler radar network. *Bull. Amer. Meteor. Soc.*, **75**, 983–994.
- Yamada, Y., and M. Chong, 1999: VAD-based determination of the Nyquist interval number of Doppler velocity aliasing without wind information. *J. Meteor. Soc. Japan*, **77**, 447–457.

